Transport and band structure studies of crystalline $ZnRh_2O_4$

Negar Mansourian-Hadavi, Supaporn Wansom, Nicola H. Perry, Arpun R. Nagaraja, and Thomas O. Mason
Department of Materials Science and Engineering, Northwestern University, Evanston, Illinois 60208, USA

Lin-hui Ye and Arthur J. Freeman
Department of Physics and Astronomy, Northwestern University, Evanston, Illinois 60208, USA

(Received 13 March 2009; revised manuscript received 20 November 2009; published 17 February 2010)

We report the synthesis and characterization of non-d^{10} *p*-type transparent conducting oxides of the normal spinel $ZnRh_2O_4$. Undoped $ZnRh_2O_4$ was successfully prepared by means of bulk solid-state synthesis. The conduction mechanism and bulk defect chemistry of polycrystalline sintered pellets of $ZnRh_2O_4$ were studied through electrical conductivity and Seebeck coefficient measurements, in defect equilibrium at elevated temperature under controlled atmospheres. Optical diffuse reflectance measurements were also carried out to evaluate band gap. The data were analyzed in terms of an activated mobility (small polaron conduction), with a hopping energy of 0.25 eV. Results from band structure calculations by LDA+U and optical band-gap measurement by UV-visible spectrometry are in good agreement with literature data.

DOI: 10.1103/PhysRevB.81.075112 PACS number(s): 71.20.−b, 72.20.Ee, 72.80.−r, 72.90.+y

I. INTRODUCTION

Virtually all commercially available transparent conducting oxides (TCOs) are *n* type; the development of a high-conductivity *p*-type TCO would be a major breakthrough, enabling advanced devices and applications (e.g., tandem solar cells, transparent transistors, etc.).[1–4] However, reported *p*-type TCOs to date suffer from significantly lower electrical conductivities (~1 S/cm) when compared to their *n*-type counterparts (for which $\sigma > 1000$ S/cm). This has been attributed to either inherent low carrier concentration or low mobility (large effective masses). The *p*-type TCOs developed thus far have involved compounds with filled *d*-shell cations, such as Ag^+ and Cu^+, otherwise known as d^{10} compounds, to avoid optical transitions in the visible involving unfilled *d* orbitals. Recently, a new generation of non-d^{10} *p*-type TCO has been introduced, taking advantage of cations such as Rh^{+3}, with filled d-t_{2g}^6 and empty d-e_g^0 levels.[5,6] It has been suggested that cations of the VIII-A family of the periodic table can exhibit a strong preference for such behavior when in octahedral coordination by oxygen. Mizoguchi *et al.* reported that the spinel compound, $ZnRh_2O_4$, exhibits *p*-type TCO behavior.[5] $ZnRh_2O_4$ is a normal spinel, with Zn in tetrahedral and Rh in octahedral sites. In this material, the *d* orbitals adopt a low spin configuration in the ground state, splitting into fully stabilized t_{2g} (sixfold degenerate) and empty e_g (fourfold degenerate) levels (Fig. 1).[7]

The band gap is therefore determined by the ligand field splitting in the subband of the metallic d^6 cation. This band gap has been measured to be in the same range as known TCOs. Mizoguchi *et al.* reported a 2.1 eV optical band gap for $ZnRh_2O_4$,[5] whereas Dekkers *et al.* reported band gaps of 2.26, 2.74, and 2.97 eV for $ZnCo_2O_4$, $ZnRh_2O_4$, and $ZnIr_2O_4$ spinel compounds, respectively, all in thin film form.[6] The electrical conductivity of these compounds is reported to be thermally activated below room temperature and to be in the range of 0.4–3.4 S/cm at room temperature.[5,6] Their *p*-type character has been confirmed by Seebeck coefficient measurements. The fabrication and properties of heteroepitaxial junctions of *p*-type $ZnRh_2O_4$ and *n*-type ZnO have recently been reported.[7]

It has also been shown that $ZnRh_2O_4$ compositions can be deposited as amorphous thin films, with *p*-type electrical properties comparable to that of their crystalline counterparts.[8,9] This has been attributed to the isotropy of the parent crystal structure (spinel) and the three-dimensional (3D) interconnectivity of its O-Rh-O octahedral network, which appears to be preserved in the amorphous state. In contrast, *p*-type TCOs based upon O-Cu-O linear bonds (e.g., in $CuAlO_2$) can be amorphized as thin films, however the bonding and the associated *p*-type properties are lost.[9] Recently, all-amorphous *p*-*n* junctions based upon the combination of *a*-$ZnRh_2O_4$ and *a*-$InGaZnO_4$ have been demonstrated.[9,10]

The crystal structure (spinel) and electronic properties (*p* type) of $ZnRh_2O_4$ have been known since the 1980s.[11,12] The work until now has been carried out at room temperature and below and exclusively on thin films. The present work was undertaken to verify the conduction mechanism of this prototype 3D *p*-type TCO by combined high-temperature transport studies of bulk ceramic specimens and first-principles electronic structure calculations.

II. PROCEDURE

A. Experimental

Bulk specimens (typically 1–2 g) of $ZnRh_2O_4$ were prepared by solid-state reaction of stoichiometric amounts of the parent oxides, ZnO and Rh_2O_3 (purity >99.9%), weighed on a Mettler balance (Mettler-Toledo, Inc., Columbus, OH,

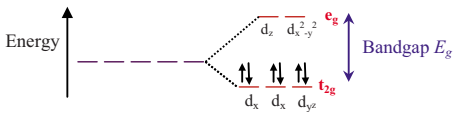

FIG. 1. (Color online) Schematic diagram of ligand field splitting for transition metal *d* orbitals.

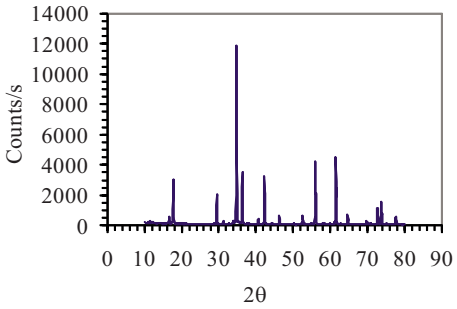

FIG. 2. (Color online) X-ray diffraction pattern for cubic $ZnRh_2O_4$ spinel phase prepared at 1200 °C in air by solid-state synthesis.

USA) with ±0.1 mg accuracy. The reagents were ground with mortar and pestle and fired in high-density alumina crucibles at 900–1100 °C in air for one day. Each sample was then ground and pressed at 125 MPa into pellets 12.5 mm diameter and ~2 mm thick. The pellets were then fired at 1200 °C over the course of 12 h and quenched in air.

The phase purity of the air-quenched polycrystalline samples was determined by x-ray powder diffraction on a Rigaku diffractometer (Rigaku, The Woodlands, TX, USA) with Ni-filtered Cu Kα radiation. Data were collected from 10° to 80° 2θ with a step size of 0.1° and a collection time of 2 s at each step. Phase purity was established by pattern-matching based on a cubic unit cell ($Fd3m$) (Fig. 2).

Simultaneous four-point dc conductivity and Seebeck coefficient measurements at temperatures from 650 to 800 °C were performed using the technique described previously.[13,14] Rectangular bar-shaped samples (approximately 3mm×3mm×9mm) were cut from sintered pellets by diamond saw and placed between Au foils, the outer electrodes for electrical measurements, with auxiliary Au wire electrode loops at ~1/3 and ~2/3 positions along the length of each bar, as described by Hong *et al.*[14] A Pt vs Pt/Rh thermocouple (type S) was placed in contact with each of the four contacts along the bar. Samples were equilibrated in air. Measurements were taken after equilibrium had been achieved (6–10 h). The measured conductivities were corrected for the porosity of the samples according to the 3D symmetric medium equation from McLachlan *et al.*[15]

$$\sigma_{measured} = \sigma_h[1 - (3/2)f], \quad (1)$$

where $\sigma_{measured}$ is the measured conductivity of the porous sample, σ_h is the conductivity of the high-conductivity (matrix) component (the conductivity we wish to measure), and f is the volume fraction of porosity. This equation is used when both phases (matrix and porosity) are interconnected in 3D. Our specimens had a relative density of ~65% (calculated from mass and pellet geometry).

Diffuse reflectance spectra of as-fired specimens were collected over a wavelength range of 200–900 nm using a Cary 500 double-beam UV-VIS-NIR spectrophotometer (Varian Instruments, Inc., Palo Alto, CA) with a lead sulfide detector and a diffuse reflectance accessory (DRA). Instrument automatically switched between tungsten and deuterium lamps for UV and visible/IR incident radiation, respectively.

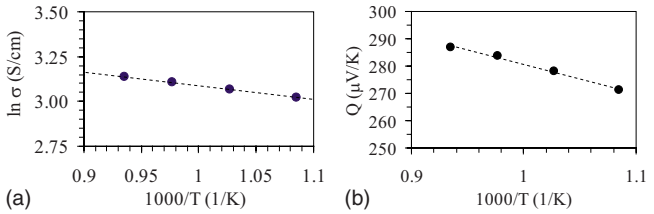

FIG. 3. (Color online) Temperature dependent behavior of (a) electrical conductivity and (b) Seebeck coefficient for $ZnRh_2O_4$ compound in air.

B. Theoretical

The electronic structure of $ZnRh_2O_4$ was calculated by the highly precise full-potential linearized augmented plane-wave (FLAPW) method[16] based on density-functional theory. The experimental[17] lattice constant of 8.506 Å was used in the present calculations. Using a theoretically optimized lattice constant instead of the experimental value resulted in only a small 0.05 eV difference in calculated band gap. The muffin-tin radii of Zn, Rh, and O atoms were chosen to be 1.89, 2.43, and 1.57 a.u., respectively. The plane-wave basis cutoff was $|k+G|<4.0$ a.u.$^{-1}$ and the star function cutoff was 9.0 a.u.$^{-1}$. Within the muffin tins, charge density and potential were expanded by lattice harmonics up to $l=8$. Brillouin-zone integration was performed by summation over the special k points of the $5\times5\times5$ Monkhorst-Pack mesh.[18] The internal parameters were optimized, followed by band structure calculations. The generalized gradient approximation[19] for structural relaxation, and LDA +U for the calculation of the band structure were used. The parameters $U=3.4$ eV and $J=0.6$ eV were taken from Stojić *et al.*[20] which were calculated by the tight-binding linear muffin-tin orbital method. Spin-orbit coupling effect was also included in the band structure via the second variational scheme.

III. RESULTS AND DISCUSSION

A. Experimental

Solid-state synthesis of $ZnRh_2O_4$ in air at 1200 °C resulted in a highly crystalline dark brown powder that was verified as phase pure by XRD analysis, as shown in Fig. 2. Scanning electron microscopy revealed an equiaxed microstructure with a grain size of ~2–3 μm.

High-temperature electrical characterization of a bar-shaped sintered ceramic specimen of $ZnRh_2O_4$ was performed in air at various temperatures (650 °C, 700 °C, 750 °C, 800 °C). The Seebeck coefficients were positive, consistent with p-type character, with absolute values ranging from +270 to +290 μV/K and increasing with temperature. These values are much larger (smaller hole contents) than those obtained by Dekkers *et al.*[6] on polycrystalline $ZnRh_2O_4$ thin films (+63 μV/K). This is not surprising since carrier contents are often much higher in thin films than in bulk materials. The temperature dependence of conductivity and thermopower are exhibited in Figs. 3(a) and 3(b), respectively. The electrical conductivity is thermally activated.

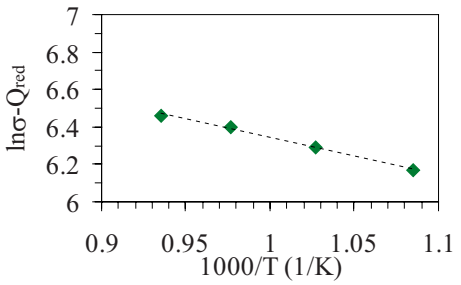

FIG. 4. (Color online) Plot of $(\ln\sigma - Q_{red})$ vs $1/T$ plot (in air) for $ZnRh_2O_4$ system, providing evidence of an activated mobility.

Conductivity is dependent on both carrier concentration (p) and mobility (μ):

$$\sigma = pe\mu, \tag{2}$$

whereas thermopower depends upon carrier concentration and the density of states in the valence band (N_v),

$$Q_+ = \frac{k}{e}\left(\ln\frac{N_v}{p} + A\right). \tag{3}$$

In these equations, e is the unit of electron charge and A is a transport constant, which depends upon the conduction mechanism. For itinerant, band-type conduction, A falls between 2 and 4, depending upon the scattering mechanism, whereas for small polaron transport, A is typically zero.[21,22]

Since the absolute value of thermopower scales inversely with logarithm of the hole content in Eq. (3), it follows that the hole concentration decreases with increasing temperature, i.e., higher absolute values are observed. In order to extract the temperature dependence of the mobility, the procedure outlined in 23 was employed. Equation (3) is rearranged to give the "reduced" thermopower, Q_{red}, which varies linearly with the logarithm of the hole content:

$$Q_{red} = -\frac{Q}{k/e} = \ln p - \ln N_v - A. \tag{4}$$

By plotting $(\ln\sigma\text{-}Q_{red})$ vs. inverse temperature, the temperature dependence of the mobility can be established from the relationship:

$$\frac{\partial(\ln\sigma - Q_{red})}{\partial 1/T} = \frac{\partial \ln\mu}{\partial 1/T}. \tag{5}$$

A more detailed analysis of mobility is given below, however the plot in Fig. 4 is strong indication of an activated mobility and small polaron conduction. A small polaron consists of the charge carrier and its associated lattice distortion or polarization. This polarization essentially traps the electronic defect at a given cation site.[24] Conduction occurs by "hopping" of the carrier and its polarization field between cations of two valence states, in this case between Rh^{4+} and Rh^{3+}. Small polaron conduction is typically associated with large carrier concentrations $(\sim 10^{21}-10^{22}/\text{cm}^3)$ and low mobilities $(<1\ \text{cm}^2/\text{V s})$.[23]

The Seebeck coefficient for small polaron is given by[23]

TABLE I. Calculated c values for $ZnRh_2O_4$ composition at their corresponding hole content, p, at various temperatures.

T (°C)	c
800	0.066
750	0.069
700	0.073
600	0.079

$$Q = \pm\frac{k}{e}\left\{\ln\left[\frac{2(1-c)}{c}\right] + A\right\}, \tag{6}$$

where A is the transport constant (usually zero for small polaron system) and c is the fraction of occupied carrier sites, which can be defined for the $ZnRh_2O_4$ spinel system as the ratio of Rh^{4+} to the total Rh species on octahedral sites:

$$c = \frac{[Rh^{4+}]}{[Rh^{3+}] + [Rh^{4+}]}. \tag{7}$$

Solving Eq. (6) for c using the experimental thermopower values obtained at various temperatures in air allows for carrier concentration to be calculated according to

$$p = Nc, \tag{8}$$

where p is the hole concentration and N is the density of conducting sites. N can be calculated knowing the cubic unit cell volume of the $ZnRh_2O_4$ spinel, 6.16×10^{-22} cm^3, and the number of rhodium cations per unit cell (i.e., 16). The resulting N value is 2.6×10^{22} cm^{-3}. Table I shows calculated c values (the fraction of octahedral sites that are Rh^{4+}). The corresponding calculated hole contents are in the vicinity of 2×10^{21} and change only slightly with temperature over the range investigated.

Absolute values of mobility can be derived from Eq. (2) based upon the carrier concentrations established on the basis of Eqs. (6)–(8). The resulting values range from 0.06 to 0.08 $\text{cm}^2/\text{V s}$, increasing with temperature (650–800 °C). Both the activated character and the low mobilities observed are indicative of small polaron conduction.

The mobility of small polaron conductors is given by[22,23]

$$\mu = \frac{g(1-c)ea^2\nu}{kT}\exp\left(\frac{-E_H}{kT}\right), \tag{9}$$

where g is the geometric factor, a is the jump distance between equivalent sites, $1-c$ is the probability that the adjacent site is the appropriate valance for exchange to occur, ν is phonon frequency, e and k are well-known constants, and E_H is defined above. Equation (9) can be re-expressed as

$$\mu = \frac{\mu_0}{T}\exp\left(\frac{-E_H}{kT}\right). \tag{10}$$

Therefore, a plot of $\ln(\mu T)$ vs inverse temperature (Fig. 5) allows for the activation energy of 0.25 eV to be determined.

We can extrapolate the data of Fig. 5 and estimate a room-temperature mobility of approximately 2.8×10^{-4}. This low

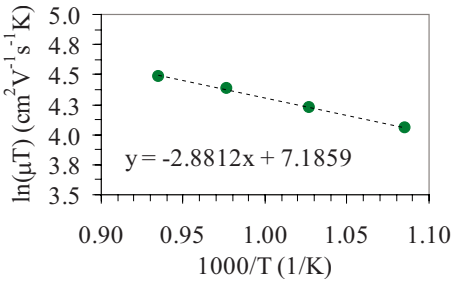

FIG. 5. (Color online) Plot of $\ln(\mu T)$ is plotted vs $1/T$ for $ZnRh_2O_4$ in air. Numbers on the data points show the raw mobility values in $cm^2/V\ s$

value may explain the observation of Dekkers *et al.* that "no significant data can be extracted from Hall measurements,"[6] owing to the combination of low mobility and such high carrier contents (e.g., $\sim 2\times 10^{21}$ cm^{-3}). From the values of c in Table I and a value of $N=2.6\times 10^{22}$ cm^{-3}, we can estimate the carrier content at room temperature ($p=Nc$) and arrive at a value for the room-temperature conductivity, of approximately 0.1 S/cm. Actual room-temperature measurements confirmed this value of conductivity.

The overall small polaron conductivity equation:[22,23]

$$\sigma = \frac{gNc(1-c)e^2a^2\nu}{kT}\exp\left(\frac{-E_H}{kT}\right) \tag{11}$$

allows for a prediction of the maximum achievable room-temperature conductivity. In the present work, values of $c\sim 0.07$ were obtained from the thermopower. By increasing c from 0.07 to 0.5, an increase in the product, $c(1-c)$, could be anticipated, which is really quite small (a factor of ~ 3.8). This is probably the most significant result of the present work, i.e., that $ZnRh_2O_4$ is limited by its small polaron mobility; without a change in conduction mechanism (e.g., small polaron to metallic), $ZnRh_2O_4$ cannot be expected to deliver the high p-type conductivities being sought. Ultimately, it is the low carrier mobility that limits conductivity in $ZnRh_2O_4$ and related spinel TCOs. [Our room-temperature conductivity of 0.1 S/cm is understandably smaller than reported thin film values (0.4–3.4 S/cm),[5,6] most likely owing to grain boundary contributions in the present work.]

The band edge was clearly visible in the diffuse reflectance spectrum, from which an optical band gap of 2.2 eV was estimated.

B. Theoretical

The LDA+U band structure and density of states of $ZnRh_2O_4$ are shown in Figs. 5(b) and 6(a), respectively. Rh $4d$ states are separated into the occupied t_{2g} and empty e_g bands, as expected, owing to the octahedral crystal-field splitting. The band gap of 1.65 eV is indirect, with the valence-band maximum (VBM) and the conduction-band minimum (CBM) being located on the $\Gamma+X$ direction and shifted from the X point. Except for the band-gap value, which was 1.0 eV larger, the LDA+U and the pure LDA band structures were very similar to each other. The fact that both the VBM and the CBM involve Rh $4d$ bands has important implications for the physical properties of $ZnRh_2O_4$. Their flat nondisperse character contribute large density of states around the Fermi level and account for the large carrier effective mass and the small polaron character (low mobility) of the electrical conductivity. It should be pointed out that the large density of states around the Fermi level suggests that $ZnRh_2O_4$ may be useful for thermoelectric applications.[25]

The accurate value of the band gap is still under debate. The earlier report of Mizoguchi *et al.*[5] gives a value of 2.0 eV. But Singh *et al.*[17] claimed that there are actually two components close to the optical absorption edge: the first corresponds to an indirect band gap of only 1.25 eV, and the second to a direct band gap of 1.8 eV. Recently, a much larger value of 2.75 eV was reported by Dekkers *et al.*[6] Theoretically, owing to the complicated electron correlation

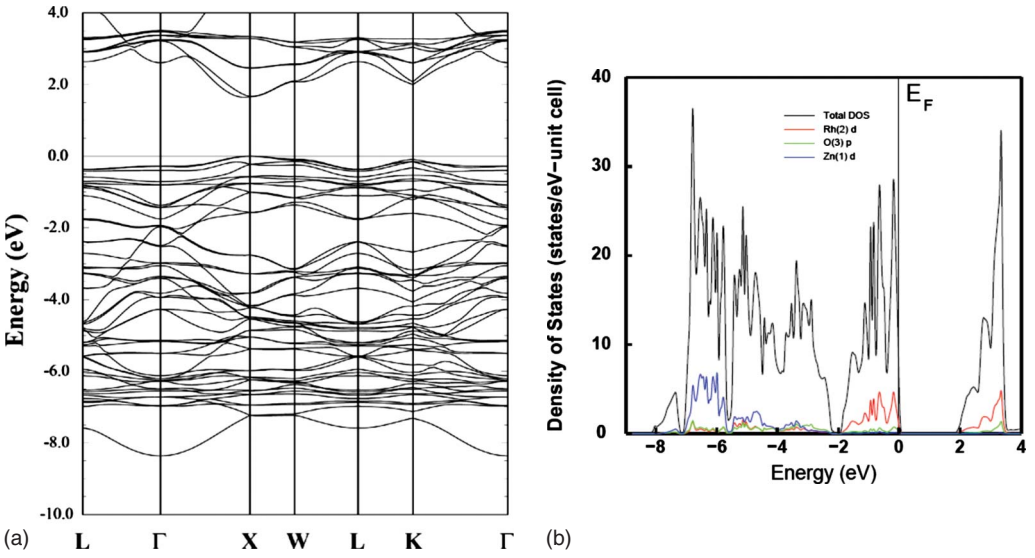

FIG. 6. (Color online) The (a) LDA+U bands and (b) density of states of $ZnRh_2O_4$

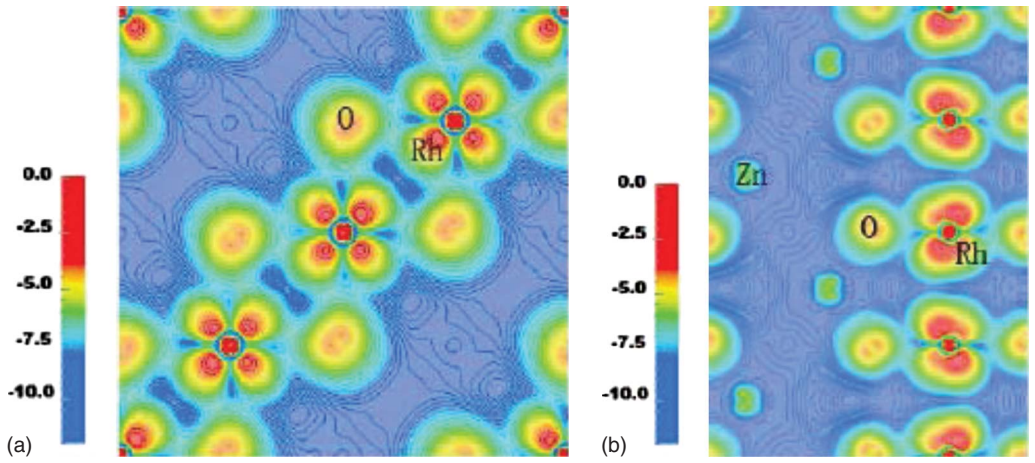

FIG. 7. (Color online) Hole density distribution of the Rh-O (001) plane (a) and the Zn-Rh-O (101) plane (b). The plot is in logarithmic scale. Holes are mostly localized on the Rh sites which also spread to the surrounding O sites. Distribution on Zn sites is negligible.

of the Rh 4*d* states, getting the accurate value of the band gap is quite difficult. Usually, LDA systematically underestimates the band gap by about 50% mainly due to its lack of the derivative discontinuity at integer electron numbers. In $ZnRh_2O_4$, however, it is argued[17] that such a systematical error of LDA should not be important: since both the VBM and the CBM share the same Rh 4*d* character, it is expected that the nonlocal effect of the electron self-energy (which is the major source of the derivative discontinuity) is small and that the LDA band gap should already compare favorably with experiment.

In reality, however, the calculated LDA band gap (0.65 eV^2) is still much smaller than all the measured values. Even in comparison with the smallest experimental gap of 1.25 eV by Singh *et al.*, the relative error of LDA is still 48%. The complexity of the band gap of $ZnRh_2O_4$ is likely related to the strong localization feature of the Rh 4*d* states, therefore calling for our LDA+U treatment, which follows the approach of Shick *et al.*[26] Indeed, the present band-gap value of 1.65 eV is in much closer agreement with experiment. The optical absorption spectrum of $ZnRh_2O_4$ (not shown) has been calculated, showing that the principle absorption edge is located at 1.8 eV which is also in reasonable agreement to our experimental result (2.2 eV).

The hole density distribution has been calculated to help us better understand the *p*-type electronic behavior of this system. In Fig. 6, the hole density is constructed by summing up the states within the small energy window of 0.1 eV below the VBM. The main feature of Fig. 7 is that the holes are mostly localized on the Rh sites, which also spread to the surrounding O owing to the Rh-O covalent bonding. Such a localization feature implies that the optic phonon modes, which alter the Rh-O bonds should strongly scatter the holes which may relate to their small polaron conducting behavior.

IV. CONCLUSION

$ZnRh_2O_4$, a prospective non-d^{10} *p*-type TCOs spinel material, was successfully synthesized by means of solid-state reactions and was characterized for its electrical and optical properties.

Analysis of the high-temperature electrical properties of $ZnRh_2O_4$ indicated an activated mobility (activation energy ~0.25 eV), indicative of small polaron conduction. Four-point conductivity and thermopower measurement were carried out in air at elevated temperatures (650–800 °C). Carrier concentrations were on the order of 10^{21} cm^{-3} and hole mobilities were less than 0.1 $cm^2\ V^{-1}\ s^{-1}$. Room-temperature conductivity was extrapolated to be on the order of 0.1 S/cm. The band gap of $ZnRh_2O_4$ was determined to be 2.2 eV by diffuse reflectance measurements.

First-principles band structure calculations indicate that Rh 4*d* states are separated into the occupied t_{2g} and empty e_g bands, as expected, owing to the octahedral crystal-field splitting. The flat nondisperse character of both the VBM and the CBM contribute large density of states around the Fermi level and account for the large carrier effective mass and the small polaron character (low mobility) of the electrical conductivity.

$ZnRh_2O_4$ has some of the requirements for *p*-type transparent conducting behavior (e.g., band gap approaching 3 eV), however the small polaron transport limits its potential conductivity. It is of interest to establish if the same mechanism governs conduction behavior in related spinel systems, such as $ZnIr_2O_4$ or $ZnCo_2O_4$. If so, a change in mechanism from small polaron transport, with its associated low carrier mobilities, will be required if spinel-based TCO materials are to be realized.

ACKNOWLEDGMENTS

This work was supported in part by the NSF MRSEC program at Northwestern University under Grant No. DMR-0520513 (theory work, high-temperature studies) and by the Center for Inverse Design, an Energy Frontier Research Center funded by the (U.S.) Department of Energy, Office of Science, Office of Basic Energy Sciences under Award No. DE-PS02-08ER15944 (structural studies, room-temperature transport). The authors are grateful to Diana Proffit for help with SEM characterization.

[1] H. Kawazoe, H. Yanagi, K. Ueda, and H. Hosono, MRS Bull. **25**, 28 (2000).
[2] A. Kudo, H. Yanagi, K. Uedo, H. Hosono, and H. Kawazoe, Appl. Phys. Lett. **75**, 2851 (1999).
[3] H. Ohta, K.-I. Kawamura, M. Orita, M. Hirano, N. Sarukura, and H. Hosono, Appl. Phys. Lett. **77**, 475 (2000).
[4] K. Tonooka, H. Bando, and Y. Aiura, Thin Solid Films **445**, 327 (2003).
[5] H. Mizoguchi, M. Hirano, S. Fujitsu, T. Takeuchi, K. Ueda, and H. Hosono, Appl. Phys. Lett. **80**, 1207 (2002).
[6] M. Dekkers, G. Rijnders, and D. H. A. Blank, Appl. Phys. Lett. **90**, 021903 (2007).
[7] P. A. Cox, *Transition Metal Oxides: An Introduction to Their Electronic Structure and Properties* (Clarendon, Oxford, 1992).
[8] H. Ohta, H. Mizoguchi, M. Hirano, S. Narushima, T. Kamiya, and H. Hosono, Appl. Phys. Lett. **82**, 823 (2003).
[9] S. Narushima, M. Mizoguchi, K.-I. Shimizu, K. Ueda, H. Ohta, M. Hirano, T. Kamiya, and H. Hosono, Adv. Mater. **15**, 1409 (2003).
[10] T. Kamiya, S. Narushima, H. Mizoguchi, K. Shimizu, K. Ueda, H. Ohta, M. Hirano, and H. Hosono, Adv. Funct. Mater. **15**, 968 (2005).
[11] I. S. Shaplygin and V. B. Lazarev, Russ. J. Inorg. Chem. **25**, 906 (1980).
[12] I. S. Shaplygin, I. I. Prosychev, and V. B. Lazarev, Russ. J. Inorg. Chem. **31**, 2870 (1986).
[13] A. Trestman-Matts, S. E. Dorris, and T. O. Mason, J. Am. Ceram. Soc. **66**, 589 (1983).
[14] B.-S. Hong, S. J. Ford, and T. O. Mason, Key Eng. Mater. **125-126**, 163 (1997).
[15] D. McLachlan, M. Blaszkiewicz, and R. E. Newnham, J. Am. Ceram. Soc. **73**, 2187 (1990).
[16] E. Wimmer, H. Krakauer, M. Weinert, and A. J. Freeman, Phys. Rev. B **24**, 864 (1981); H. J. F. Jansen and A. J. Freeman, *ibid.* **30**, 561 (1984).
[17] D. J. Singh, R. C. Rai, J. L. Musfeldt, S. Auluck, N. Singh, P. Khalifah, S. McClure, and D. G. Mandrus, Chem. Mater. **18**, 2696 (2006).
[18] H. J. Monkhorst and J. D. Pack, Phys. Rev. B **13**, 5188 (1976).
[19] J. P. Perdew, K. Burke, and M. Ernzerhof, Phys. Rev. Lett. **77**, 3865 (1996).
[20] N. Stojić, N. Binggeli, and M. Altarelli, Phys. Rev. B **73**, 100405(R) (2006).
[21] A. F. Joffe, *Physics of Semiconductors* (Infosearch Ltd., London, 1960).
[22] H.-C. Chen, E. Gartstein, and T. O. Mason, J. Phys. Chem. Solids **43**, 991 (1982).
[23] J. Nell, B. J. Wood, S. E. Dorris, and T. O. Mason, J. Solid State Chem. **82**, 247 (1989).
[24] M. W. Barsoum, *Fundamentals of Ceramics*, 2nd ed. (I. O. P. Publishing, Bristol, 2003), p. 203.
[25] G. B. Wilson-Short, D. J. Singh, M. Fornari, and M. Suewattana, Phys. Rev. B **75**, 035121 (2007).
[26] A. B. Shick, A. I. Liechtenstein, and W. E. Pickett, Phys. Rev. B **60**, 10763 (1999).